Numerical simulations of water-air-bubble mixed flows around hydrofoil and propeller

Numerical simulations of water-air-bubble mixed flows around hydrofoil and propeller

Tianyi Mao, Xinyi Li and Decheng Wan*

Computational Marine Hydrodynamics Lab (CMHL), School of Naval Architecture, Ocean and Civil Engineering, Shanghai Jiao Tong University, Shanghai, China
*Corresponding author: dcwan@sjtu.edu.cn

Abstract. Water-air-bubble mixed flow is a complex multiphase flow usually generated due to the intense interaction between the sailing ship and the free surface[1].A large number of bubbles scour down along the ship which gather around the propulsion system, making a significant effect on the hydrodynamic performance of propeller and hydrofoil. In this paper, the hydrodynamic performance of two-dimensional hydrofoil and three-dimensional propeller in uniformly mixed water-air-bubble incoming flow is studied by using the Computational Fluid Dynamics (CFD) method. Euler-Euler two-fluid model is used to simulate the uniformly mixed water-air-bubble incoming flow with the open-source CFD software OpenFOAM. The feasibility of numerical simulation is verified by comparing the numerical simulation results with experimental data. On this basis, the changes of physical fields around two-dimensional hydrofoil and three-dimensional propeller caused by water-air-bubble flow under multiple air fraction conditions are discussed. In addition, the differences in dimensionless coefficients are compared between single-phase flow conditions and two-phase flow. Furthermore, the Population Balance Model (PBM) is used in the simulation of two-dimensional hydrofoil to observe the coalescence and break of bubbles.

1. Introduction

Water-air-bubble mixed flow is a complex flow which will be generated when ships or marine engineering structures interact with the surrounding fluid. It usually involves air, water and a large number of bubbles with different sizes. In the water-air-bubble mixed flow, lots of bubbles will sweep down from bow to the stern. Also, the whirlpool turbulence in the stern of the ship will suck in a large amount of gas, which also produce water-air-bubble mixed flow. The bubbles cluster near the propulsion system, which leads to the unreliability of hydrodynamic performance, resistance performance and propulsion performance forecast. Under the condition that the similarity rule between the actual scale structures and models is still unclear, it is difficult to predict the hydrodynamic performance of marine structures or ships by experiments. Therefore, it is particularly important to adopt highly reliable numerical simulation methods to study the force situation of water-air-bubble mixed flow around the ships and analyze the effect.

Nowadays, the numerical simulation methods have been adopted to the water-air-bubble mixed flow. The numerical simulation methods can be divided into two types—Interface capture model and Non-interface capture model. Non-interface capture model mainly includes Euler-Lagrange method, and Euler-Euler method. And the Interface capture model mainly includes Volume of Fluid Method (VOF)[2], Level-Set method. Euler-Lagrange method defines bubbles as tiny particles in the flow[3].So

it can track the bubbles through the Lagrange method and solve the two phase based on Euler method. The Euler-Lagrange method simulates collisions between bubbles. However, this method requires large amount of calculation which costs lots of time and computing resources. Euler-Euler method solves the two-phase flow problems by N-S equation based on Euler mesh. It views all the discrete bubbles in the flow as a continuous fluid and it can't analyse the movement of each bubble. Since the discrete phase is solved in Euler mesh, the velocity of different particles in the mesh is considered to be the same. So the Euler-Euler method only needs small amount of calculation, and gives the results quickly. In the traditional Euler-Euler method, we can't consider the coalescence and fragmentation of bubbles. So the PBM is introduced into the method to consider the coalescence and fragmentation of bubbles. Some studies apply PBM to investigate the skin-friction drag reduction on a flat plate with bubble injection[4]. It is difficult to use interface capture method or Euler-Lagrange method. This paper uses the Euler-Euler method to model the water-air-bubble mixed flow.

2. Simulation background

2.1. Governing Equations

In the Eulerian-Eulerian two-fluid solution framework, the governing equations including the mass conservation equation and the momentum conservation equation are solved separately for each phase. When simulating, the liquid phase is considered as the continuum phase and the gas phase is taken as the dispersed phase. In this paper, the two phases are both regarded as incompressible flows which are immiscible, and the heat transfer between phases is neglected.

The mass conservation equation and the momentum conservation equation are as follows :

$$\frac{\partial}{\partial t}(\alpha_i \rho_i) + \nabla \cdot (\alpha_i \rho_i \boldsymbol{u_i}) = 0 \tag{1}$$

$$\frac{\partial}{\partial t}(\alpha_i \rho_i \boldsymbol{u_i}) = -\nabla \cdot (\alpha_i \rho_i \boldsymbol{u_i u_i}) - \alpha_i \nabla p - \nabla \cdot \left[\alpha_i \mu_i \left(\nabla \boldsymbol{u_i} + \nabla \boldsymbol{u_i^T}\right)\right] + \alpha_i \rho_i g + \boldsymbol{F_{ij}} \tag{2}$$

where the subscript i represent the phase, in which i = l or g means the water phase or air phase respectively. **u** is velocity, p is pressure, g is the gravity acceleration ρ is density, and α represents the volume fraction.

$\mathbf{F_{ij}}$ means the interphase force between gas and liquid phases, mainly used to represent the momentum transfer between phases, which is combined with various forces as follows:

$$\boldsymbol{F_{ij}} = \boldsymbol{F_D} + \boldsymbol{F_L} + \boldsymbol{F_{WL}} + \boldsymbol{F_{TD}} + \boldsymbol{F_{VM}} \tag{3}$$

$\mathbf{F_D}$ stands for drag force, which is caused by the relative motion between the gas and liquid phases. $\mathbf{F_L}$ stands for lift force, the lateral force caused by the pressure difference perpendicular to the direction of the bubble's motion. $\mathbf{F_{WL}}$ stands for wall lubrication force, which is generated by the slip velocity near the wall. $\mathbf{F_{TD}}$ is the turbulent diffusion force, and represents the traction force caused by liquid turbulence on the bubble. $\mathbf{F_{VM}}$ stands for virtual mass force is the one generated by bubbles' acceleration in the water. Here we only take the drag force and virtual force into account when simulating hydrofoil and all interphase forces are considered for propeller.

In this paper, F_D is calculated as:

$$\boldsymbol{F_D} = -\frac{\mathbf{1}}{\mathbf{2}} \boldsymbol{C_D \rho_l |u_r| u_r A_d} \tag{4}$$

where C_D is the drag coefficient, ρ_l is liquid density,u_r is the relative velocity between two phases which can be calculated as $\boldsymbol{u_g - u_l}$, and A_d is the projected area of the bubble.

Nowadays, drag models such as Schiller-Naumann model, Grace model, Ishii-Zuber model and Tomiyama model have been widely used in numerical simulation of water-air-bubble mixed flow, and have been implanted in commercial CFD software for users to choose. In this paper, we choose the drag force model proposed by Schiller[5]for the two dimensional hydrofoil and the drag force model proposed by Ishii[6] for the three dimensional propeller.

The virtual mass force F_{VM} can be calculated as:

$$\boldsymbol{F_{VM}} = C_{VM}\alpha_g\rho_l \cdot \left(\frac{D\boldsymbol{u_g}}{Dt} - \frac{D\boldsymbol{u_l}}{Dt}\right) \tag{5}$$

where the total derivate is defined as:

$$\frac{D}{Dt} = \frac{\partial}{\partial t} + \boldsymbol{u}\cdot\boldsymbol{\nabla} \tag{6}$$

C_{VM} is the coefficient of virtual mass force which is always be regarded as a constant in most related literatures. So in this paper, bubbles are considered as spheres and C_{VM} is taken as 0.5.

The lift force $\boldsymbol{F_L}$ is calculated as:

$$\boldsymbol{F_L} = -\boldsymbol{C_L\rho_l\alpha_g u_r}\times(\boldsymbol{\nabla}\times\boldsymbol{u_l}) \tag{7}$$

where C_L is the lift coefficient and similar to drag models, different lift models which mainly focuses on the lift coefficient can be choosen in CFD softwares. The lift model proposed by Tomiyama[7] is adopted here.

The wall lubrication force $\boldsymbol{F_{WL}}$ can be described as:

$$\boldsymbol{F_{WL}} = C_{WL}\frac{\rho_l\alpha_g}{d_b}\boldsymbol{u_{rw}^2 n_w} \tag{8}$$

where C_{WL} represents the wall lubrication force coefficient, u_{rw} represents the tangential component of relative velocity at the wall and $\boldsymbol{n_w}$ represents the external unit normal vector on the wall. The Antal wall lubrication force model[8] is used here.

For the turbulent diffusion force, current turbulent diffusion force model can be divided into two categories:Lopez de Bertodano model and Favre-averaged-drag model. The former supposes that the bubble motion approximates the thermal diffusion of air molecules in atmosphere and is applied here as follows:

$$\boldsymbol{F_{TD}} = -C_{TD}\rho_l k_l \nabla\alpha \tag{9}$$

where k_l represents the turbulent kinetic energy of the liquid phase. The turbulent diffusion coefficient C_{TD} usually ranges from 0.1 to 1.0, and it is a constant 1.0 here.

2.2. Population balance model

In the real environment, the merging and breaking of bubbles are very common, which leads to the multi-scale distribution of bubble size. Also because bubble size distribution will change with the interphase transfer phenomenon in the polyphase system, using the Population-Balance-Model to describe the distribution of bubbles of different sizes in the liquid phase has become a hot topic in the field of gas-liquid two-phase flow.

The transport equation considering bubble collapse and coalescence can be described as:

$$\frac{\partial}{\partial t}\big(n(V)\big) + \nabla\cdot\big(\boldsymbol{u}n(V)\big) + \nabla\cdot\big(G_v n(V)\big) = B_A + D_A + B_B + D_B \tag{10}$$

where G_v represents the growth rate of bubbles, B_A and D_A are the production and disappearance terms related to bubble merging.

$$B_A = \frac{1}{2}\int_0^V \Gamma_c(V-V',V')n(V-V')\,n(V')dV' \tag{11}$$

$$D_A = \int_0^\infty \Gamma_c(V,V')n(V)n(V')dV' \tag{12}$$

B_B and D_B are the production and disappearance terms related to bubble breaking, V represents the volume of sub-bubbles after crushing and n(V) is the bubble number density function of volume V.

$$B_B = \int_{\Omega_V} p\,g_b(V')\beta_b(V|V')n(V')dV' \tag{13}$$

$$D_B = g_b(V)n(V) \tag{14}$$

where V' represents the bubble volume before breakin, $g_b(V')$ is breaking frequency, $\beta_b(V|V')$ is the probability density function of bubble breakage, $\Gamma_c(V,V')$ is bubble coalescence rate.

The coalescing models generally require collision frequency and coalescing-efficiency-model to describe the coalescing frequency, and the crushing models are generally expressed as models of bubble-breaking frequency and sub-bubble size distribution.

Various coalescing-and-crushing models have been created to simulate the merging and breaking of bubbles. In this paper, the coalescing-and-crushing model proposed by Luo[9] is applied to the PBM.

3. Numerical simulation of hydrofoil

3.1. Calculation conditions

A two-dimensional NACA0012 hydrofoil profile is taken as the research object in this paper. The setting of velocity and angle of attack of the NACA0012 hydrofoil profile is based on the experiment of the same type of hydrofoil profile in single-phase incoming water flow conditions[10]. The geometric model of the hydrofoil profile is set as Figure 1 and the parameters are set as Table 1.

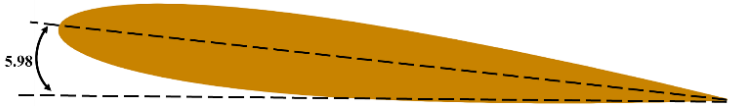

Figure 1. Geometric model of the hydrofoil profile.

Table 1. Parameters of calculation conditions.

Parameters	Unit	Value
Attack angle of hydrofoil	degree	5.98
Chord length of hydrofoil L	m	1
Velocity of incoming flow	m/s	2.24
Kinematic viscosity of water	m2/s	1.12×10^{-6}
Kinematic viscosity of air	m2/s	1.46×10^{-5}
Re		200 000

In the first model, the bubble is assumed to have a constant diameter. The diameter is set as 0.5 mm. The volume fraction of air is set as 0%, 5%, and 10%.

3.2. Computational domain

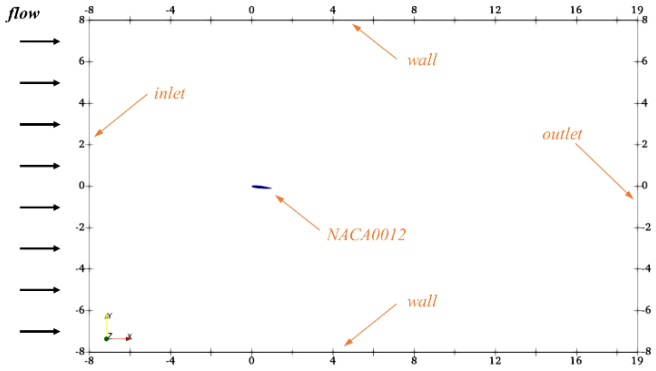

Figure 2. General layout of computational domain.

The general layout of the computational domain is set in Figure 2. This paper applies the oxy system. L is the chord length of the hydrofoil. The length of the domain is set from -8L to 19L and the direction is set along the x-axis. The inlet boundary is located at x=-8L. The outlet boundary is located at x=19L. The width of the domain is set from -8L to 8L and the direction is set along the y-axis. So the distance between the hydrofoil profile and the fixed boundary can be considered large enough to avoid the far-field effect.

The water-air-bubble mixed flow is generated at the inlet boundary and propagates along the x-positive direction.

3.3. Mesh distributions

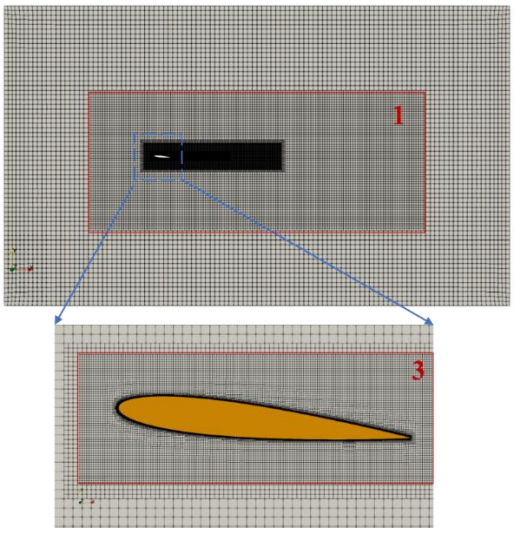

Figure 3. The mesh of computational domain.

This paper applies the mesh by the software Hexpress. The mesh distribution is set in Figure 3. The mesh division is to apply block densification near the hydrofoil profile based on the background grid. Two boxes are applied, as shown in the Figure 3, to densify the background mesh at level 1 and level 3 in the specific location.

The layer thickness of the boundary layer of the hydrofoil profile is limited to $y^+<10$, and the layer thickness of the first boundary layer is 0.00012 m. The total number of meshes is 72885.

The timestep is calculated through Courant number (Co) value as follows:

$$Co = \frac{\Delta t|\boldsymbol{U}|}{\Delta x} < 1 \tag{15}$$

where Δt is the timestep size, $|\mathbf{U}|$ is the modulus of velocity, and Δx is the length of the cell along the velocity direction.

3.4. Boundary conditions

The incoming flow is set at the inlet boundary. The velocity boundary condition is set as $\boldsymbol{u_l} = \boldsymbol{u_g} = \boldsymbol{u}_\infty$. The fixed value boundary condition is applied for α_g and α_l. The pressure condition is set according to the fixedFluxPressure condition in OpenFoam. The turbulent kinetic energy k, turbulence specific dissipation rate ω and the turbulence viscosity ν_t is calculated as in equation (16-18).

$$k = \frac{3}{2}(I|\boldsymbol{u}|)^2 \tag{16}$$

$$\omega = \frac{k^{0.5}}{C_\mu^{0.25} l} \tag{17}$$

$$v_t = \frac{a_1 k}{max(a_1\omega, SF_2)} \tag{18}$$

where I is the turbulence intensity, C_μ and a_1 are empirical constants. ($C_\mu = 0.09$, $a_1 = 0.31$), and l is the turbulent reference length scale.

At the outlet boundary, the velocity boundary applies the zero normal gradient condition. The pressure condition is set at fixed value. The inlet and Outlet boundary condition is applied for α_g, α_l,k, and ω. The turbulence viscosity ν_t is calculated as in equation (18).

At the hydrofoil boundary, the velocity boundary applies no-slip boundary condition. And the pressure condition applies the zero normal gradient condition. It also goes for volume fraction and ω. For k and ν_t.

3.5. *Model validation*

This paper validates the numerical model in single-phase incoming water flow conditions. The numerical results of lift and drag coefficients are compared with experimental results. The lift and drag coefficients are calculated through the following formulas.

$$C_L = \frac{F_{lift}}{\frac{1}{2}\rho_l \boldsymbol{u}_\infty{}^2 L} \tag{19}$$

$$C_D = \frac{F_{drag}}{\frac{1}{2}\rho_l u_\infty{}^2 L} \tag{20}$$

where F_{lift} and F_{drag} are lift and drag forces of the hydrofoil profile.

Table 2. Comparison of C_L and C_D between experiment and numerical model.

Condition	CL	Cd
Experimental results	0.6084	0.0134
Pure water environment	0.6338	0.0130
Error	2.54%	2.99%

In Table 2, the lift and drag coefficients calculated in this paper are compared with the experimental results. The error is less than 3%. Based on the table, the numerical model in this paper conforms to the experimental results. So the model is validated.

4. Numerical simulation of propeller

4.1. Geometric Model and Computational Domain

The geometry of the propeller is the KP505 propeller model. The propeller diameter D is 0.25m, the rotate speed of the propeller is 9.5 r/s. and other geometric features are shown in the Figure 4.

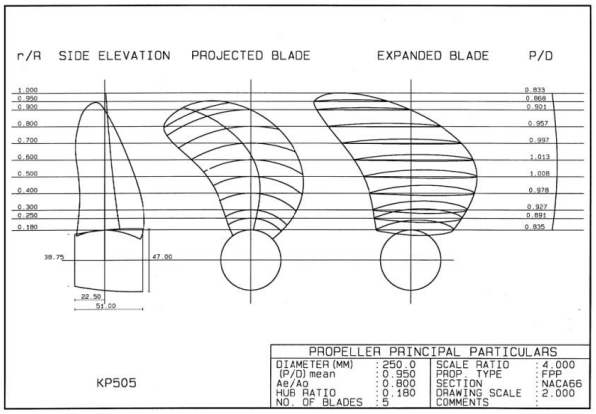

Figure 4. The Geometric model of propeller.

The general layout of the computational domain is shown in Figure 5. To simulate an open deep water environment, this paper takes the computational domain as a box with a cross-section of a square whose side length is equal to 4D, where D means the propeller diameter. The length of this rectangular body is 8D, and the distance from the inlet and outlet to the propeller are both 4D which is far enough to prevent unexpected disturbance from the boundary. In this field, the Cartesian coordinate o-xyz system is adopted and the origin is set at the center of the propeller. The x-axis is along the length of propeller, while the y and the z-axes both are along the radial direction of the propeller.

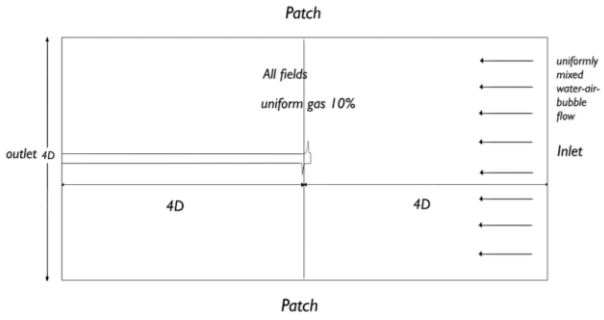

Figure 5. General layout of computational domain.

In this paper, the bubble in water-air-mixed flow is assumed to be spherical and has a constant diameter. $d = 0.1\text{mm}$. The coalescence and break-up of bubbles are not considered in this paper. The volume fraction of air is set as 10% and the volume fraction of water is set as 90% at the inlet and in the computational domain. At the initial moment, the water-air-mixed-flow was assumed that it has already filled the entire computational domain which means the propeller starts rotating in a uniformly mixed water-air-flow to improve the stability of the simulation and to reduce time costs. And the uniformly mixed water-air-bubble incoming flow also is generated at the inlet where x=-4D and flows forward along the x-positive direction.

4.2. Mesh Distributions and time step

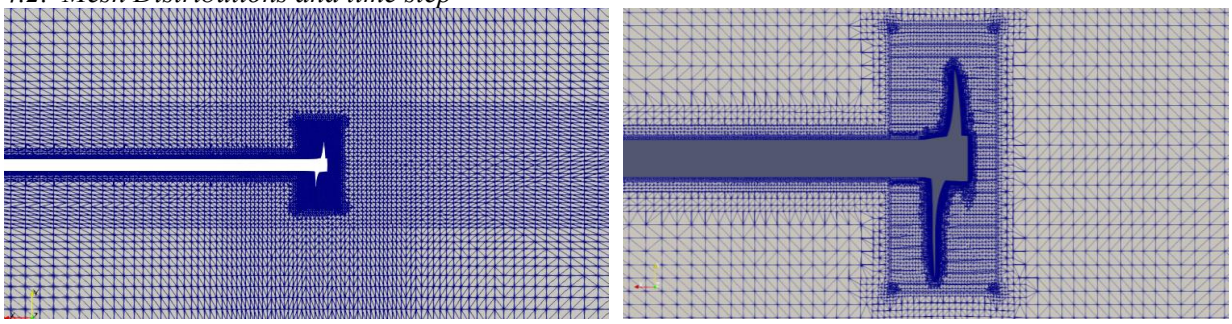

(a) the overall meshes. (b) magnified view of partial meshes.

Figure 6. The mesh of computational domain.

In this paper, the mesh is generated by the preprocessing code snappyHexMesh in OpenFOAM, which is in the form of unstructured mesh. The overall mesh distribution are shown in Figure 6(a) and partial meshes around the KP505 propeller is shown in Figure 6(b).

The background mesh is a gradient mesh with a gradual change ratio of 4 along x-axis and 2 along the y and z-axis. The mesh around the propeller and in the rotating area is much finer than that elsewhere not only for capturing the details of the propeller motion but also to save computational resources. The first layer thickness of the boundary layer near the propeller is about 0.0001m and the stretching ratio is 1.4. The y^+ ranges from 30 to 70. The total number of mesh is 982171.

The timestep size is determined based on a prescribed Courant number (Co) value as follows:

$$Co = \frac{\boldsymbol{u}\Delta t}{\Delta x} \leq 1.5 \tag{21}$$

where Δt is the timestep size, u is the normal velocity, and Δx is the distance between the cell centre and the centre of its neighbour cell.

4.3. Boundary conditions

At the inlet, $\boldsymbol{u_g}$ and $\boldsymbol{u_w}$ use the fixed value condition which equals 1.665m/s, α_g and α_l also take the fixed value condition which is 0.1 and 0.9 respectively. For the pressure, the fixedFluxPressure condition is adopted. The initial value of the turbulent kinetic energy k and turbulence-specific dissipation rate ω are calculated as follows:

$$k = 1.5(I|\boldsymbol{u}|)^2 \tag{22}$$

$$\omega = \frac{k^{0.5}}{C_\mu^{0.25} l} \tag{23}$$

where I means turbulence intensity, C_μ is a constant equals to 0.09 and l is the turbulent reference length scale.

At the outlet, the fixed value which equals 0 is used for the pressure boundary condition, and the zerogradient condition is applied to velocity and volume fraction. The inletOutlet boundary condition is applied to α_g, α_l, k and ω.

On the propeller boundary，moving wall velocity condition is used for $\boldsymbol{u_l}$ and $\boldsymbol{u_g}$ to adapt the rotation of the propeller awe, and no-slip boundary condition is used for the propeller shaft. The zero normal gradient condition is adopted for pressure, volume fraction and the wall function method is for k and ω .

On the patch boundary, fixed value boundary condition, zero gradient condition is used for all scalars and vectors.

In this paper, the rotation of the propeller is achieved through sliding mesh called AMI, the boundary for the AMI is cyclicAMI applied to all scalars and vectors.

4.4. Validation and verification

In this research, simulation of the propeller is conveyed under the condition that advance ratio J=0.7 and is validated in single-phase incoming water flow conditions. The numerical results about thrust coefficient K_T, moment coefficient K_Q and open water efficiency $\eta_0$are compared with experimental data.

Advance ratio J, thrust coefficient K_T, moment coefficient $\mathrm{K_Q}$ and openwater efficiency η_0 are shown as follows:

$$J = \frac{V_A}{Dn} \tag{24}$$

$$K_T = \frac{T}{\rho n^2 D^4} \tag{25}$$

$$K_Q = \frac{Q}{\rho n^2 D^5} \tag{26}$$

$$\eta = \frac{J}{2\pi}\frac{K_T}{K_Q} \tag{27}$$

where n is propeller rotating speed, T is thrust, Q is moment, D is the propeller diameter, V_A is incoming flow velocity and ρ is the density of water.

Table 3. Comparison between Numerical results and Experimental results.

Results	K_T	$10K_Q$	η_0
Numerical results	0.1897	0.3008	0.703
Experimental results	0.1850	0.3110	0.665
Error between Numerical results and Experimental results	2.54%	3.28%	5.65%

From the Table 3, the error between numerical results and experimental results are all below 6%, which is acceptable for propeller numerical simulation. On the basis of the comparison, the numerical model established in this paper agrees with the experimental results.

5. Results and discussion

5.1. Results and discussion of hydrofoil

5.1.1. Comparison of flow fields

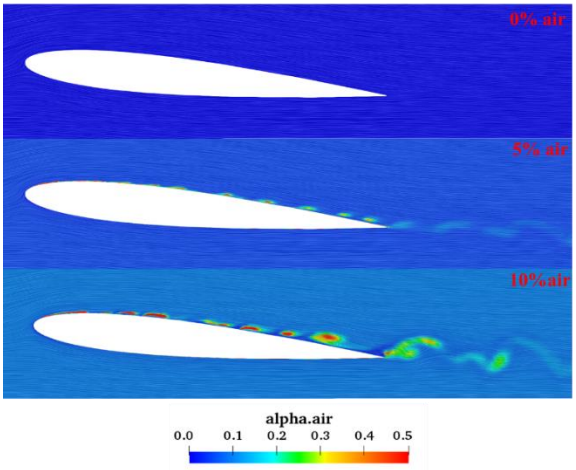

Figure 7. Air volume fraction distribution and LIC streamline distribution near the hydrofoil.

Figure 7 shows the air volume fraction, near the hydrofoil in water-air-bubble mixed flow conditions at different α_g. The LIC is also adopted to visualize the streamline. From the fig, the distribution of air volume is different on the suction surface and the pressure surface. The suction surface of the hydrofoil has higher air volume fraction and the change is more distinct than the pressure surface.

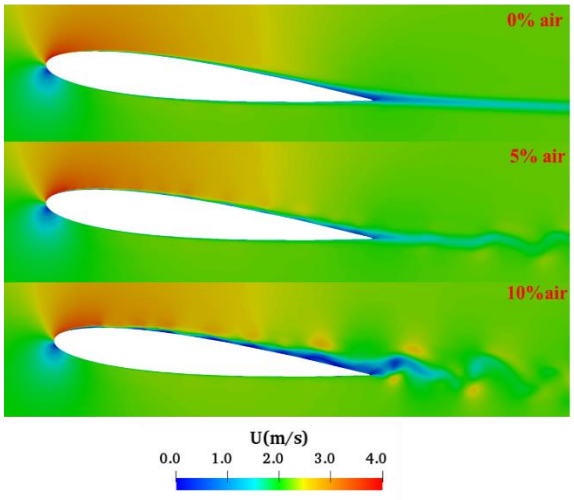

Figure 8. The velocity field near the hydrofoil.

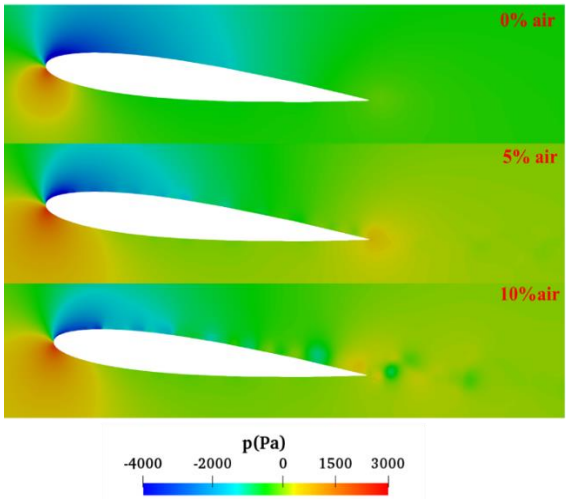

Figure 9. The pressure field near the hydrofoil.

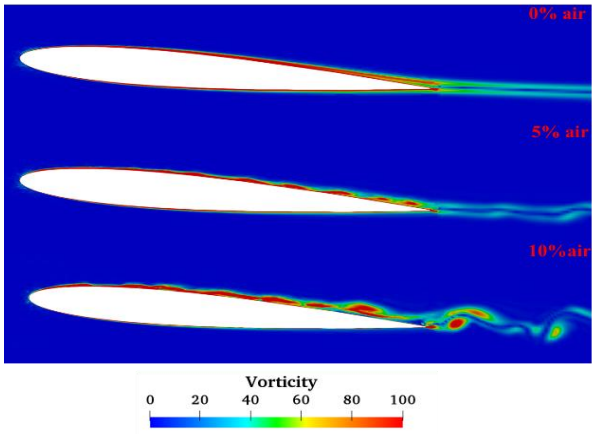

Figure 10. The vortex structure near the hydrofoil.

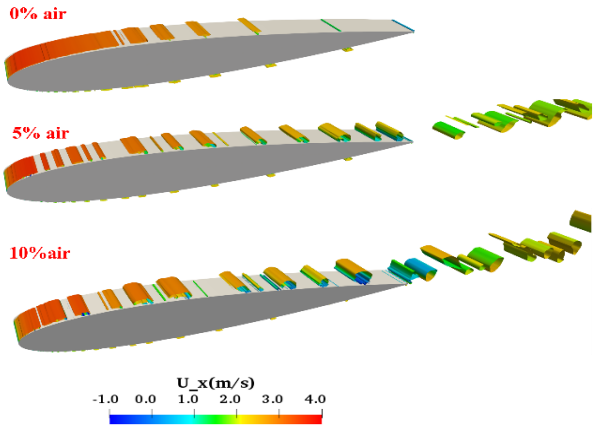

Figure 11. The vorticity near the hydrofoil.

Figure 11 shows the vorticity near the hydrofoil. Figure 10 shows the vortex structure near hydrofoil extracted from the third generation vortex recognition method Liutex The vortexes are generated and propagated along with higher air volume fraction. Also, the phenomenon of vortexes is more obvious in the condition of water-air-bubble mixed flow.

5.1.2. Comparison of drag and lift coefficients

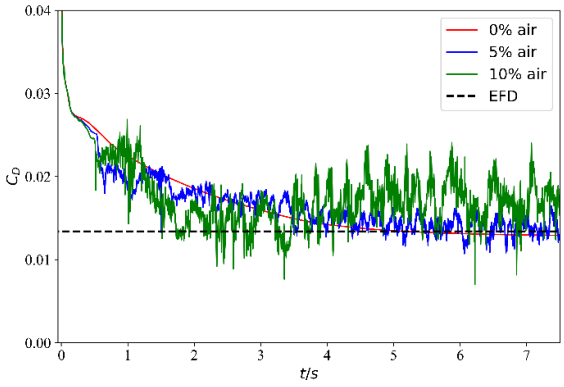

Figure 12. Comparison of time history of lift coefficient C_D.

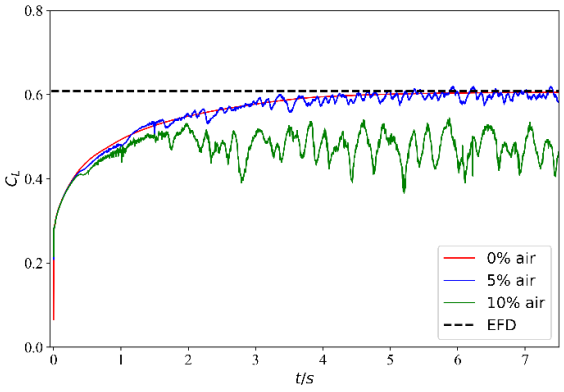

Figure 13. Comparison of time history of lift coefficient C_L.

Table 4. Comparison of average C_L and C_D.

Condition	C_L	C_D
0% air in incoming flow	0.6338	0.0130
5% air in incoming flow	0.5884	0.0142
10% air in incoming flow	0.4744	0.01733

This paper calculates the average C_L and C_D from t=5s to t=8s. Table 4 shows the results. One can see that the lift coefficient decreases and the drag coefficient increases with the increasing of α_g.

5.1.3. Population balance model

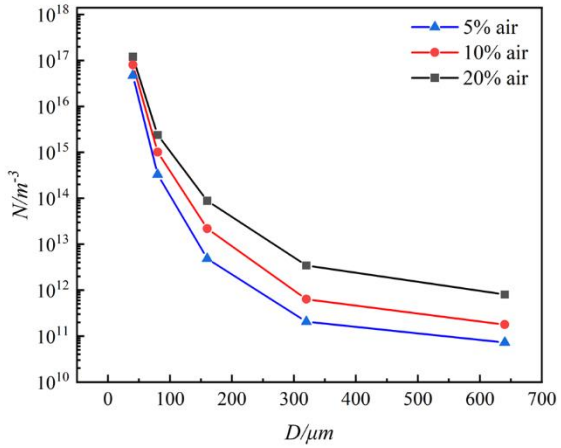

Figure 14. The bubble number density distribution

In this study, 5 bubble diameter groups were selected: $D_0 = 640\mu$m、$D_1 = 320\mu$m、$D_2 = 160\mu$m、$D_3 = 80\mu$m、$D_4 = 40\mu$m. Relevant studies show that: if the logarithm of the bubble radius in micrometers is taken as the horizontal mark and the logarithm of the number of bubbles in a certain radius is taken as the ordinate of the water body per cubic meter, then all bubbles are located in the linear strip area with a slope of -10/3. So the relationship between the initial volume fraction rate of the 5 groups of bubbles can be deduced: $f_0 = 0.1218, f_1 = 0.1523, f_2 = 0.1904, f_3 = 0.2380, f_4 = 0.2975$.

Figure 9 shows the bubble number density distribution in the flow field at t=7s. We can observe that, for different values of α_g, the tendency of bubble aggregation and fragmentation is the same, and that higher values of α_g result in the production of more large-diameter bubbles.

5.2. Results and discussion of propeller

5.2.1. Comparison of propeller performance

To take the error into consideration, two-phase results are compared with single-phase results instead of the standard open water experimental results.

Table 5. Comparison between single phase results and two-phase results

Results	K_T	$10K_Q$	η_0
Single Phase results	0.1897	0.3008	0.703
Two Phase results	0.1663	0.2739	0.677
Decrease between Single Phase results and two-phase results	12.33%	8.96%	3.70%

From the Table 5, it can be found that thrust coefficient K_T, moment coefficient K_Q and openwater efficiency η_0 have decreased by 12.33%, 8.96% and 3.70% respectively in the water-air mixed flow of 0.1 α_g. The decrease in thrust coefficient exceeds 10% and is too huge to be neglected. It reveals the fact that the existence of air affects thrust more than moment and that propeller performance will decrease obviously if it is put in the water-air-mixed flow of high air volume fraction like 10%.

5.2.2. Propeller Static Pressure

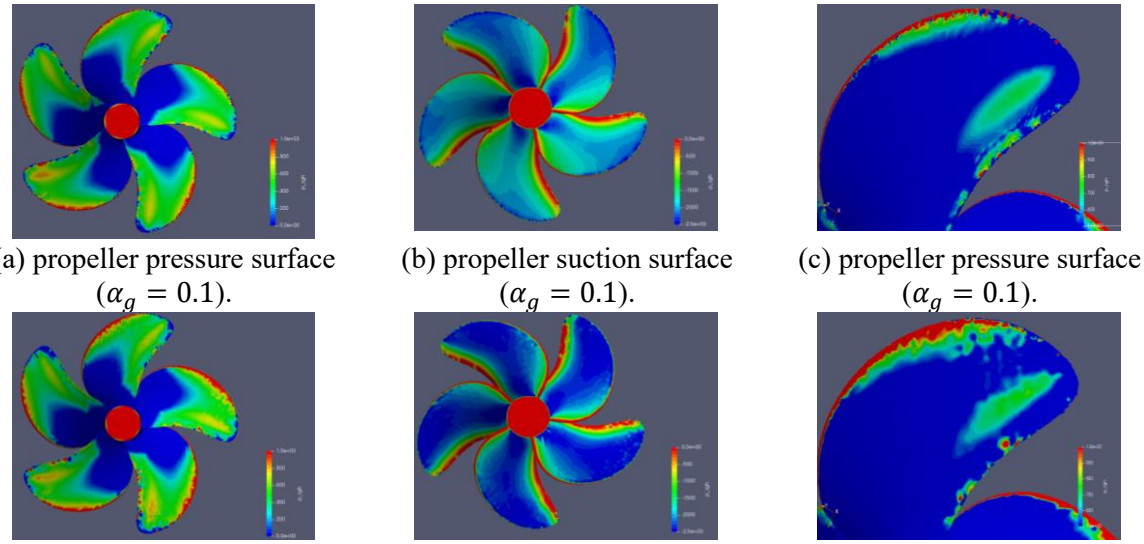

(a) propeller pressure surface ($\alpha_g = 0.1$). (b) propeller suction surface ($\alpha_g = 0.1$). (c) propeller pressure surface ($\alpha_g = 0.1$).

(d) propeller pressure surface ($\alpha_g = 0$). (e) propeller suction surface ($\alpha_g = 0$). (f) propeller pressure surface ($\alpha_g = 0$).

Figure 15. The pressure distribution of propeller.

In Figure 15(a) and Figure 15(d) shows that on the pressure surface, there is little significant difference in pressure distribution between the condition of $\alpha_g = 0$ and $\alpha_g = 0.1$. But at the tip of the blade, it can be found that high static pressure ranges wider in pure water than in water-air-mixed flow. Also, this means the pressure gradient under $\alpha_g = 0.1$ is huger than that under $\alpha_g = 0$, thus leading to the decrease of η_0 and K_Q. According to the research results of Kawakita[11], there is also some similar conclusion. On the suction surface of the propeller, the pressure distribution changes much more obvious. When $\alpha_g = 0.1$, the absolute value of static pressure is lower than that under $\alpha_g = 0$. This leads to the thrust deduction because it is the difference of static pressure between two surfaces that generate the thrust.

5.2.3. Comparison of Flow Fields

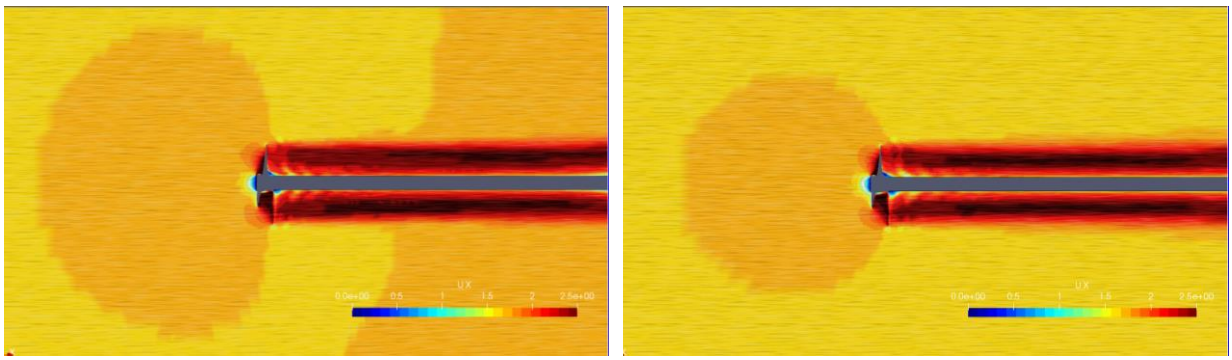

(a) water-air-bubble mixed flow condition. (b) single-phase incoming water flow condition.

Figure 16. The velocity field near the hydrofoil propeller

Figure 16 shows the comparison of instantaneous velocity field, comparing with single-phase incoming water flow, the existence of a bubble intensifies the asymmetry of the flow field. Furthermore, there is a velocity augment in the propeller wake when $\alpha_g = 0.1$.

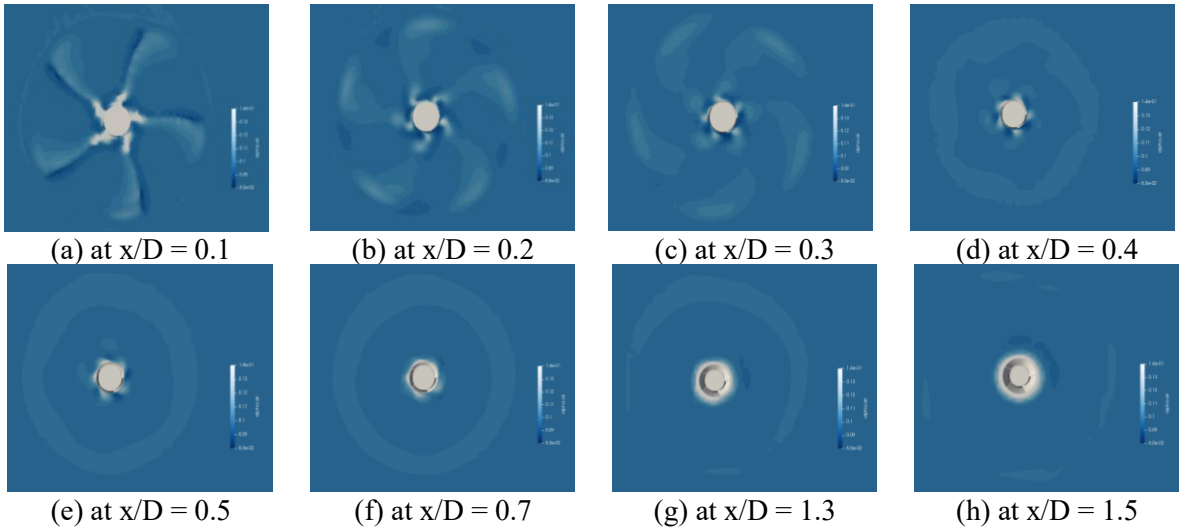

(a) at x/D = 0.1 (b) at x/D = 0.2 (c) at x/D = 0.3 (d) at x/D = 0.4

(e) at x/D = 0.5 (f) at x/D = 0.7 (g) at x/D = 1.3 (h) at x/D = 1.5

Figure 17. Instantaneous air volume fraction distribution at t=1s

The Figure 17 reflects the evolution process of bubbles in the propeller wake flow field. From the above figures, it can be seen that at a distance of 0.1D from the propeller (a)， the gas gathering in the water presents a clear blade shape, and the bubbles mostly accumulate at the blade root and blade trailing edge, while the gas content decreases at the blade guide edge. This phenomenon corresponds to the pressure distribution of the propeller blades, indicating that the gas accumulation phenomenon in the propeller wake flow field is caused by the pressure distribution on the propeller. The gas is compressed from high-pressure region to low-pressure region, and then is influenced by the propeller induced-velocity, rotating and diffusing towards the surrounding area. As the distance from the propeller increases, the shape of the coalesced gas gradually changes from the blade (a b c) to a circle (e f). Finally, the coalesced gas disappears (g h), and the air volume fraction in this area returns to uniformly mixed 0.1.

6. Conclusions

In this paper, the effects of uniformly mixed water-air-bubble incoming flow on hydrodynamic performance and fields characteristic of hydrofoil and propeller has been studied. Eulerian-Eulerian two-fluid solution framework is adopted to simulate the uniformly-mixed water-air-bubble multiphase incoming flow. Validation of simulation is conducted by comparing previous experimental and numerical results in single-phase incoming flow with numerical results in this paper, and come to a conclusion that numerical model established here is precise enough to imitate the motion of hydrofoil and propeller.

The differences caused by the mixed water-air-bubble multiphase flow on the flow field, lift and drag coefficients are discussed in hydrofoil simulation. The number density of bubble modeled by PBM is also discussed. And the variations of the static pressure distribution, flow field and performance coefficients are studied in propeller simulation.

Main conclusions about hydrofoil are summarized as follows:

- Air volume on suction surface of the hydrofoil is higher and the change is more distinct than the pressure surface.
- The existence of bubble causes fluctuation in flow field of hydrofoil, and with the increase of α_g, the fluctuation and instability are more obvious.
- The phenomenon of vortexes is more obvious at the condition of water-air-bubble mixed flow.

- With the increasing of air volume fraction, the oscillation of lift and drag coefficient tends to be more obvious and the lift coefficient decreases and the drag coefficient increases with the increasing of α_g.
- The increasing of α_g leads to the generation of more large diameter bubbles.

Main conclusions about propeller are summarized as follows:

- The existence of air causes decreases in hydrodynamic performance of propeller.
- High static pressure of pressure surface ranges wider in pure water than in water-air-mixed flow, the pressure gradient is huger in water-air-mixed flow than in pure water, the absolute value of static pressure on suction surface when bubble exist is lower than that in pure water.
- The existence of a bubble intensifies the asymmetry of the flow field.
- The static pressure on propeller influences the bubble distribution in propeller wake field.

Acknowledgements
This work was supported by the National Natural Science Foundation of China (52131102), and the National Key Research and Development Program of China (2019YFB1704200), to which the authors are most grateful.

References

[1] Li, Z., Zhang, X. S., and Wan, D. 2022 Research progress on the hydrodynamic performance of water-air-bubble mixed flows around a ship *J. Hydrodyn*. 34(2) pp 171-188
[2] Hirt, C.W., and Nichols, B.D. 1981 Volume of Fluid (VOF) Method for the Dynamics of Free Boundaries *J. Comput. Phys*. 39 pp 201–225
[3] Zhang, X., Wang, J., and Wan, D. 2020 An Improved Multi-Scale Two Phase Method for Bubbly Flows *Int. J. Multiphas. Flow* 133 p 103460
[4] Qin, S., Chu, N., Yao, Y., Liu, J., Huang, B., and Wu, D. 2017 Stream-wise distribution of skin-friction drag reduction on a flat plate with bubble injection *Phys. Fluids* 29(3) p 037103
[5] Schiller, L. and Naumann, A. 1935 A Drag Coefficient Correlation *Zeit Ver. Deutsch. Ing*. 77 pp 318-320
[6] Ishii, M., and Zuber, N. 1979 Drag coefficient and relative velocity in bubbly, droplet or particulate flows *Aiche J.* 25(5) pp 843-855
[7] Tomiyama, A. , Kataoka, I. , Zun, I. , and Sakaguchi, T. 2008 Drag coefficients of single bubbles under normal and micro gravity conditions *Jsme Int. J.* 41(2) p 472
[8] Antal, S., Lahey, R., and Flaherty, J. 1991 Analysis of phase distribution in fully developed laminar bubbly two-phase flow *Int. J. Multiphas. Flow* 17(5) pp 635-652
[9] Luo, H., and Svendsen, H. 1996 Theoretical model for drop and bubble breakup in turbulent dispersions *Aiche J.* 42(5) pp 1225-1233
[10] Shang, Y., and Horrillo, J.J., 2021. Numerical Simulation and Hydrodynamic Performance Predicting of 2 Two-Dimensional Hydrofoils in Tandem Configuration *J. Mar Sci. Eng.* 9 p 462
[11] Kawakita, C. 2013 Study on marine propeller running in bubbly flow *In Proceedings of the Third International Symposium on Marine Propulsors* 13 pp 405-411